Physics Letters A 384 (2020) 126775

Contents lists available at ScienceDirect

Physics Letters A

www.elsevier.com/locate/pla

First principle investigation of H_2Se, H_2Te and PH_3 sensing based on graphene oxide

Ehab Salih [a], Ahmad I. Ayesh [a,b,*]

[a] Department of Mathematics, Statistics and Physics, Qatar University, P. O. Box 2713, Doha, Qatar
[b] Center for Sustainable Development, Qatar University, P. O. Box 2713, Doha, Qatar

ARTICLE INFO

Article history:
Received 12 May 2020
Received in revised form 16 July 2020
Accepted 26 July 2020
Available online 3 August 2020
Communicated by M. Wu

Keywords:
Graphene oxide
Charge transfer
Gas sensor
Adsorption energy
DFT

ABSTRACT

Detecting toxic gases is of great importance to protect our health and preserve the quality of life. In this work, graphene (G) and graphene oxide with three different modifications (G–O, G–OH, and G–O–OH) have been used to detect hydrogen selenide (H_2Se), hydrogen telluride (H_2Te), and phosphine (PH_3) molecules based on Atomistic ToolKit Virtual NanoLab (ATK-VNL) package. The adsorption energy (E_{ads}), adsorption distance (D), charge transfer (ΔQ), density of states (DOS), and band structure have been investigated to confirm the adsorption of H_2Se, H_2Te, and PH_3 on the surface of G, G–O, G–OH, and G–O–OH systems. The results of G revealed highest E_{ads} for the case of H_2Te with −0.143 eV. After the functionalization of G surface, the adsorption parameters reflected an improvement due to the presence of the functional groups. Particularly, the highest adsorption energy was found between G–O system and H_2Se gas with E_{ads} of −0.319 eV. The smallest adsorption distance was found between G–OH system and H_2Se gas. The highest charge transfer was found for the case of H_2Se gas adsorbed on G–O–OH system. By thorough comparison of the adsorption energy, adsorption distance, and charge transfer between G, G–O, G–OH, and G–O–OH systems and the three gases, G–O–OH system can be considered as a potential sensor for H_2Se gas.

1. Introduction

The great improvements in industry and technology in recent decades turned the quality of life to be much easier than before in ancient times. Nevertheless, these improvements are associated with the release of some unuseful substances in forms of solids, liquids, and toxic gases that affect negatively our health [1,2]. The existence of toxic gases in air even at low concentrations is a serious problem for all the creatures on the earth [3]. For instance, the colorless H_2Se gas is a highly toxic and flammable with unpleasant strong smell at room temperature that can be generated by reaction of hydrogen gas and selenium or by reaction of selenide with acids [4,5]. The presence of H_2Se gas on air would cause serious damages to eyes and lungs [6,7]. H_2Te, on the other hand, can be generated in natural gas and crude petroleum, and it may be generated through decomposition that occur for organic matter. It is a colorless gas with the same structure of H_2Se and its existence in air may last for a while and can be easily smelled as rotting garlic at low concentrations. However, it smells like rotting leeks at the high concentration. Moreover, PH_3 is a toxic gas used mainly in agriculture to overcome the existence of insects, it is also utilized in silicon device fabrication as a dopant, and used for fabrication of phase change catalysts as well as ligands [8]. Over breathing of PH_3 gas would affect seriously the lungs which results in pulmonary edema, headache, vomiting, and tightness in chest [9]. Consequently, the improvement of low cost, accurate, and highly sensitive gas sensors is of great importance. Hence, a considerable trend of research has been published in the recent decades on the investigation of either experimental or theoretical gas sensors with high sensitivity [10–19].

Carbon based nanomaterials (C-NMs) have been subjected, in recent years, to intensive investigations due to their incredible electronic, magnetic, and optical properties, as well as their chemical versatility and biocompatibility [20,21]. Form the different types of C-NMS, graphene and its derivatives have been extensively investigated in the field of sensors, thanks to their outstanding characteristics such as good thermal stability, high chemical strength, high carrier mobility, and enormous surface area [22–26]. Nevertheless, graphene showed some limitations in the field of

* Corresponding author at: Department of Mathematics, Statistics and Physics, Qatar University, P. O. Box 2713, Doha, Qatar.
E-mail address: ayesh@qu.edu.qa (A.I. Ayesh).

https://doi.org/10.1016/j.physleta.2020.126775

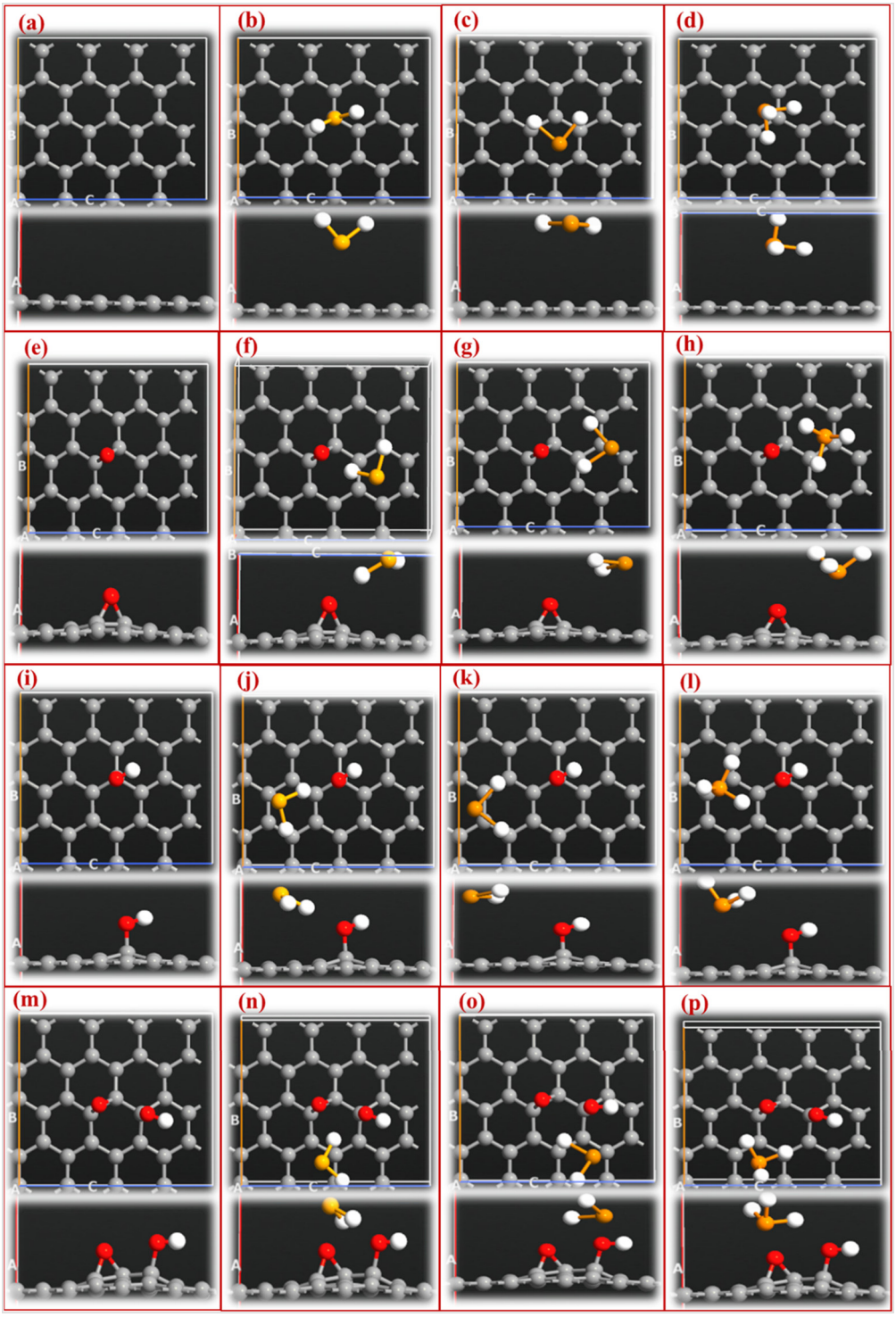

Fig. 1. Top and side views of the optimized structures of: a) G, b) G–H_2Se, c) G–H_2Te, d) G–PH_3, e) G–O, f) G–O–H_2Se, g) G–O–H_2Te, h) G–O–PH_3, i) G–OH, j) G–OH–H_2Se, k) G–OH–H_2Te, l) G–OH–PH_3, m) G–O–OH, n) G–O–OH–H_2Se, o) G–O–OH–H_2Te, and p) G–O–OH–PH_3.

sensors due to some drawbacks including its zero band gap, difficulty of attaining high quality for mass production, and the lack of functional groups on its surface [27]. Different techniques could be used to overcome these limitations including the generation of graphene that exhibits a controllable band gap and functionalizing its surface with various functional groups [27,28]. Among the various forms of graphene, graphene oxide (GO) revealed a significant performance for sensing applications, thanks to its stimulating mechanical and electrochemical characteristics, ease of its large scale production, and the possibility to introduce chemically active defects as well as functional groups on its surface [29–32]. Researchers demonstrated that the surface properties, structure, and dispersion of GO structures in epoxy matrix can be controlled by adjusting the content of functional groups that contain oxygen [33]. Furthermore, carboxyl group can be used for the generation of reactive oxygen species that is related closely with epoxide/hydroxyl [34]. The existence of functional groups on the surface of GO has been reported to be the reason for enhancing the perfor-

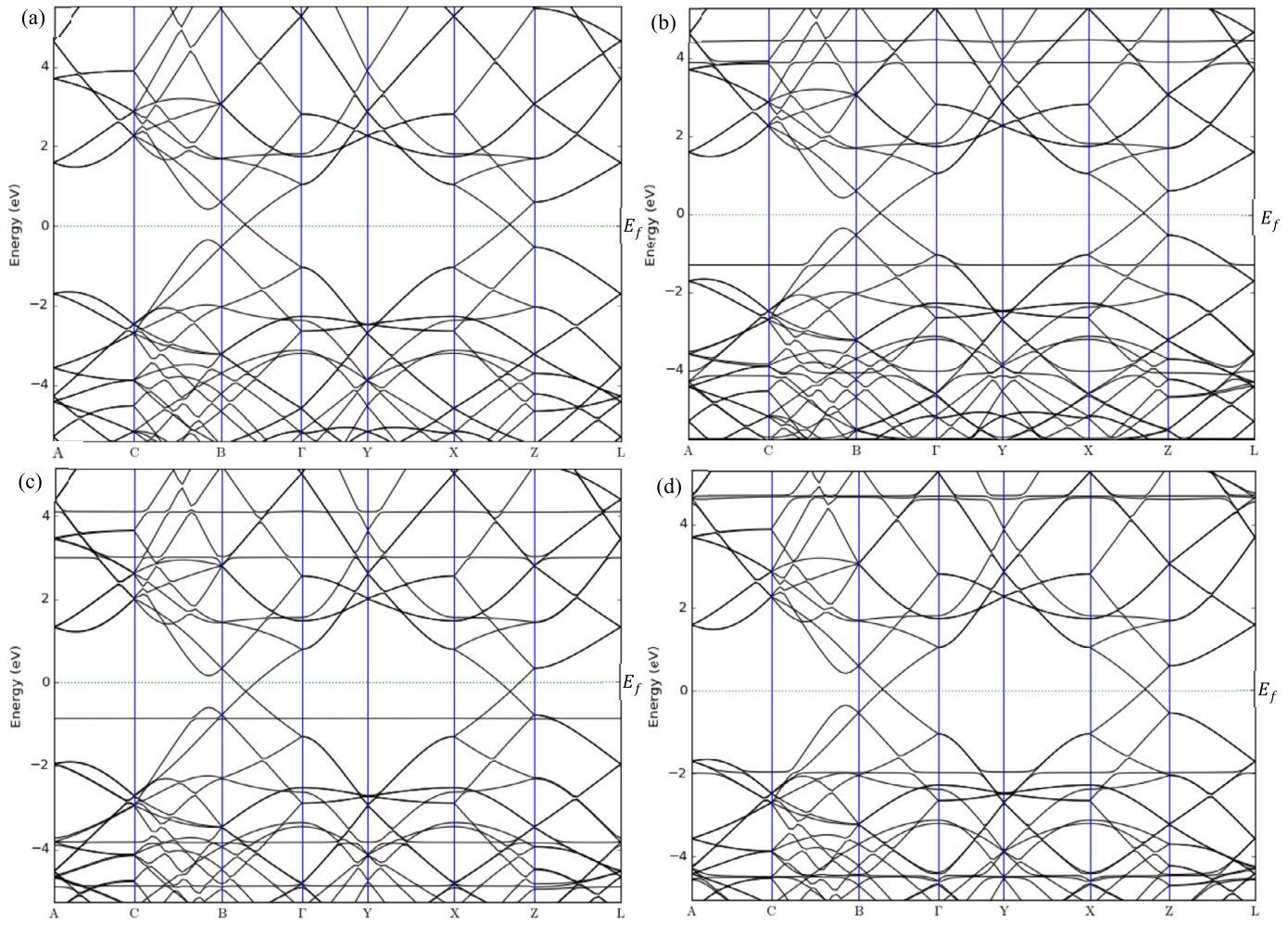

Fig. 2. Band structures of a) G, b) G–H_2Se, c) G–H_2Te, and d) G–PH_3.

mance of GO for gas sensor applications by serving as a potential adsorption sites for the gas molecules [26,35–37].

Different experimental studies have been reported in the recent years about using GO based materials in the field of gas sensors. For example, GO was prepared using ac dielectrophoresis process and then utilized to detect hydrogen gas [38]. The researchers of this study demonstrated that GO based sensor has a sensing response of 5% and fast recovery time of (<60 s) at room temperature. In another study GO was investigated experimentally as NO_2 gas sensor and the results was confirmed using first principles calculations [39]. In this study, both the experimental and theoretical calculations reflected that GO could be utilized as an effective gas sensor thanks to the reversible and high response at room temperature.

In the study reported herein, graphene based sensors were built using density functional theory (DFT) with the aid of Atomistic ToolKit Virtual NanoLab (ATK-VNL) package and then used to detect H_2Se, H_2Te, and PH_3 molecules. The surface of G has been then functionalized with an epoxy (–O–) and a hydroxyl (–OH) groups to create three different forms of graphene oxide: G–O, G–OH, and G–O–OH. The results showed that graphene is capable to adsorb the three gases. Moreover, an improvement in the adsorption parameters has been observed for cases of graphene oxide (G–O, G–OH, and G–O–OH), thanks to the presence of the functional groups which allowed the ease of adsorption of the gases.

Table 1
Adsorption energy, adsorption distance, and charge transfer of the optimized H_2Se, H_2Te, and PH_3 molecules adsorbed on G and the three forms of GO.

System	E_{ads} (eV)	D (Å)	Q (e)
G–H_2Se	−0.105	3.52	−0.010
G–O–H_2Se	−0.319	2.28	−0.081
G–OH–H_2Se	−0.244	2.19	−0.097
G–O–OH–H_2Se	−0.265	2.39	−0.113
G–H_2Te	−0.143	3.83	−0.006
G–O–H_2Te	−0.166	3.37	−0.011
G–OH–H_2Te	−0.170	3.49	−0.026
G–O–OH–H_2Te	−0.186	2.73	−0.047
G–PH_3	−0.118	3.41	−0.011
G–O–PH_3	−0.116	3.38	−0.009
G–OH–PH_3	−0.124	3.19	−0.011
G–O–OH–PH_3	−0.140	3.05	−0.035

2. Computational method

Graphene and three different functional forms of GO (G–O, G–OH, G–O–OH) have been investigated in the current study by DFT calculations based on ATK-VNL package. The four generated systems have been used as gas sensors to detect H_2Se, H_2Te, and PH_3 molecules. All systems and gas molecules have been initially optimized and fully relaxed until convergence of force to 0.01 eV/Å and most stable adsorption configuration were attained. For the exchange correlation functional, the generalized gradient approximation (GGA) combining with the Perdew-Burke-Ernzerhof (PBE)

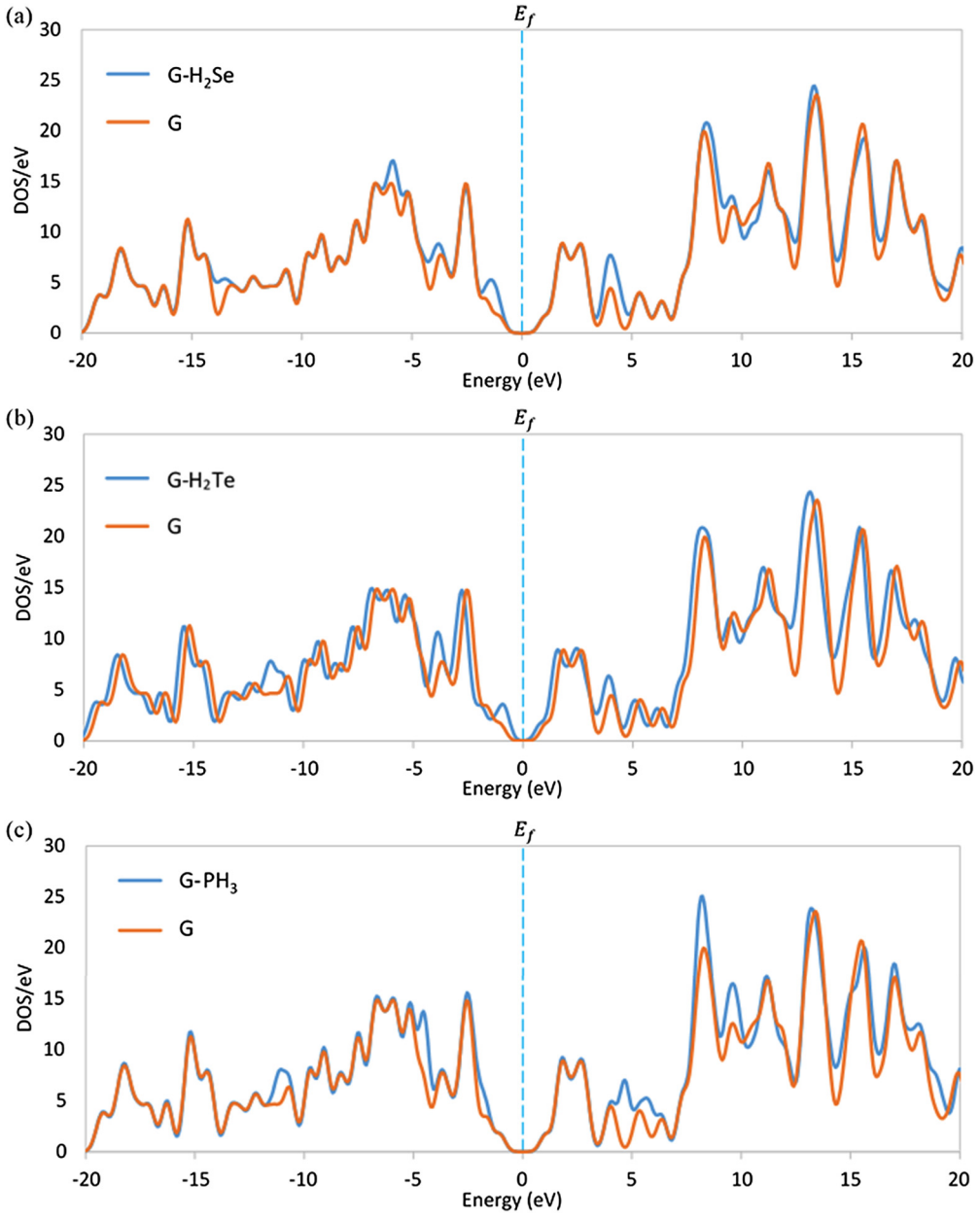

Fig. 3. Density of states of G prior and after the adsorption of a) H_2Se, b) H_2Te, and c) PH_3.

has been used [40,41]. A density mesh cutoff of 125 Hartree has been used during all calculations. $4 \times 4 \times 1$ k-point sampling was set through Monkhorst–Pack method [42]. The adsorption energy (E_{ads}), adsorption distance (D), charge transfer (ΔQ), band structure, and density of states (DOS) have been studied to confirm the detection of H_2Se, H_2Te, and PH_3 molecules. The following formula has been used to calculate the adsorption energy between the gas molecules and the four systems [43–45].

$$E_{ads} = E_{G/GO+gas} - (E_{G/GO} + E_{gas}) \quad (1)$$

Where $E_{G/GO+gas}$ is the total energy of the optimized structure of any gas molecules adsorbed on any of G, G–O, G–OH, and G–O–OH systems. $E_{G/GO}$ is the total energy of any of the four systems without the gas adsorption, and E_{gas} is the total energy of each optimized gas: H_2Se, H_2Te, and PH_3. Increasing the adsorption energy with negative sign reflects more stable configuration as well as a stronger adsorption of H_2Se, H_2Te, and PH_3 molecules on the surfaces of G, G–O, G–OH, and G–O–OH systems [1,29]. Furthermore, charge transfer of H_2Se, H_2Te, and PH_3 molecules have been evaluated using Mulliken population analysis [46,47].

3. Results and discussion

3.1. Graphene

The unmodified G is firstly used to detect H_2Se, H_2Te, and PH_3 molecules. The G, G–H_2Se, G–H_2Te, and G–PH_3 systems are initially optimized to attain the most stable adsorption configuration as shown in Figs. 1(a)–1(d). After optimization, the length of the C–C bond of G is found to be 1.43 Å. To confirm the adsorption of H_2Se, H_2Te, and PH_3 molecules on the surface of G, the adsorption energy, adsorption distance, as well as charge transfer have been calculated and listed in Table 1. The results reveal that the adsorption energy of H_2Te on G is the highest with E_{ads} of −0.143 eV. While, the adsorption distances between H_2Se, H_2Te, and PH_3 molecules and G are 3.52, 3.83, and 3.41 Å, respectively.

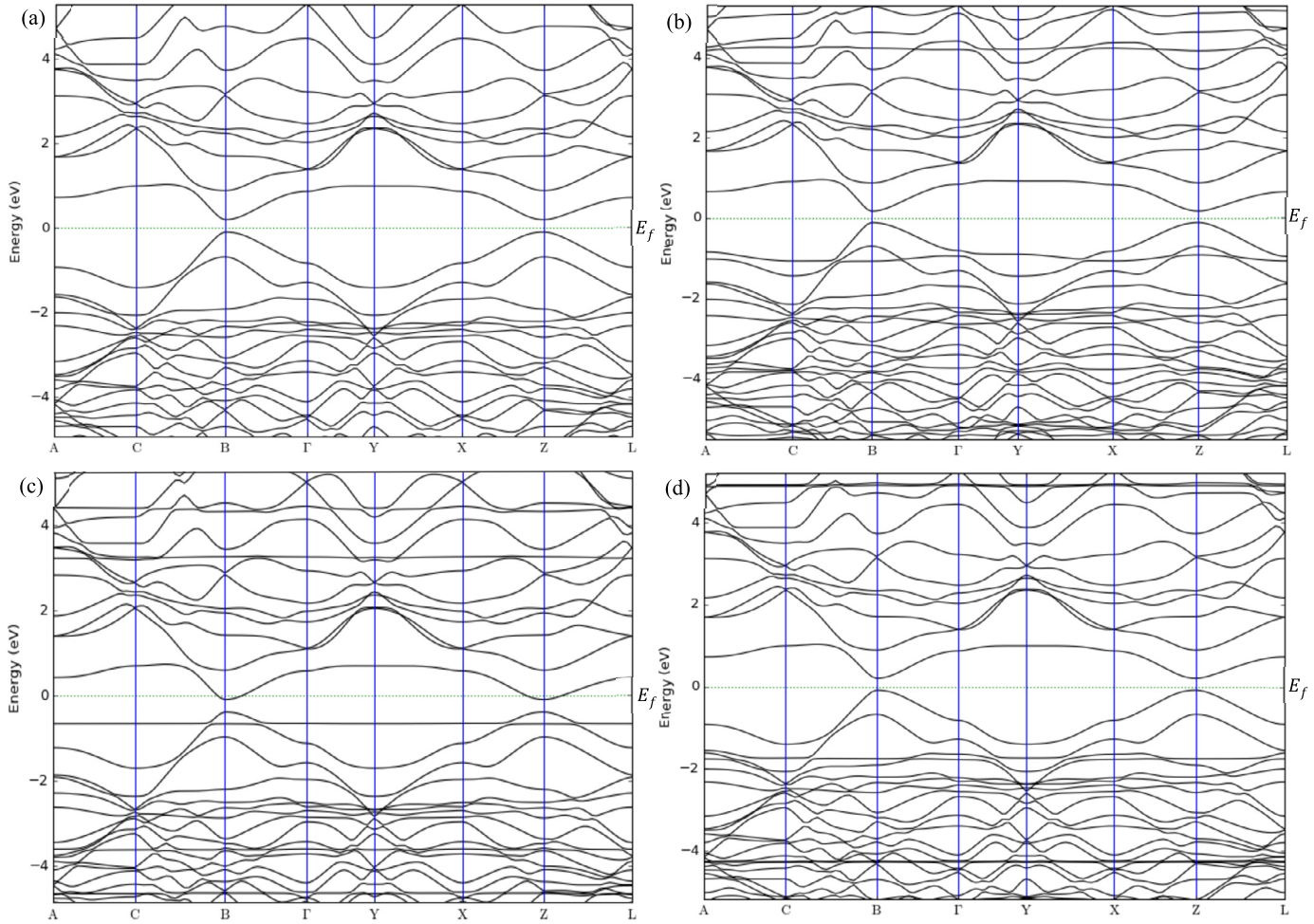

Fig. 4. Band structures of a) G–O, b) G–O–H_2Se, c) G–O–H_2Te, and d) G–O–PH_3.

Moreover, the charge transfer analysis shows that −0.010, −0.006, and −0.011 e transfer between H_2Se, H_2Te, and PH_3 molecules and G, respectively, during the adsorption process. Figs. 2(a)–2(d) show the band structures of G prior and after the adsorption of H_2Se, H_2Te, and PH_3 molecules. The results reveal that the band gap of G (Fig. 2a) is zero which is in agreement with the reported values [48,49]. Furthermore, the intersection points between the valence and the conduction bands, that are known as Dirac points, match the Fermi level which is an original feature of pure graphene [49]. Although, no changes are observed in the band gap after the adsorption of H_2Se, H_2Te, and PH_3 molecules; some changes and new bands are detected under and above Fermi level confirming the adsorption process. The density of states of G prior and after the adsorption of H_2Se, H_2Te, and PH_3 molecules are shown in Figs. 3(a)–3(c). The DOS at Fermi level is zero for the cases of G and G–H_2Se, G–H_2Te, and G–PH_3. Nevertheless, considerable increase in DOS around −5.8, −3.8, and 4.1 eV after the adsorption of H_2Se is observed (Fig. 3(a)) reflecting that more states are accessible to be occupied which confirms the adsorption of H_2Se on the surface of G [50]. Moreover, the two peaks around −1.6 and −0.8 eV disappear and a new peak around −1.2 eV is observed instead. In the case of H_2Te adsorbed on G (Fig. 3(b)), a new peak appears around −11.3 eV and a considerable increase in the DOS at around −3.8, −0.8 and 4.1 eV are detected as well, which verify the adsorption of H_2Te on the surface of G. Moreover, a significant increase of DOS around −10.7, −4.4, 5.7, 8.2, and 9.7 eV, as well as a new peak around 4.7 eV, are observed upon adsorption of PH_3.

3.2. Functionalization with epoxy group (G–O)

To improve the sensitivity of G towards the detection of H_2Se, H_2Te, and PH_3 molecules, its surface is modified with one –O– group to create the first form of GO (G–O). After optimization, the C–O bond of GO–O is 1.46 Å, while the C–C bond length around the epoxy increases to 1.5 Å as shown in Figs. 1(e)–1(h). The adsorption parameters of the optimized H_2Se, H_2Te, and PH_3 molecules adsorbed on G–O have been then calculated and shown in Table 1. The results show a significant improvement in the adsorption parameters of G after the functionalization with –O– group for the case of H_2Se. For instance, the adsorption energy increases to −0.319 eV indicating stronger adsorption of the gas on the surface of G–O as compared with pure G. Moreover, the adsorption distance decreases to 2.28 Å, and the charge transfer increase significantly to −0.081 e. The significant improvement in the adsorption parameters of G upon functionalization with the –O– group denotes an improvement in the sensitivity of G–O [50]. The band structures of G–O prior and after the adsorption H_2Se, H_2Te, and PH_3 molecules have been also investigated and shown in Figs. 4(a)–4(b). Fig. 4(a) shows that the band gap of G–O increases to 0.292 eV due to the presence of the –O– group which is in good agreement with the reported literature [27,51]. The band gap of G–O then decreases to 0.282 and 0.289 eV upon the adsorption of H_2Se and PH_3 molecules, respectively. After the adsorption of H_2Te (Fig. 4(c)), a new band is observed near the Fermi level giving it a zero band gap indicating an improvement in the conductivity of G–O due to the adsorption of the gas molecule. The

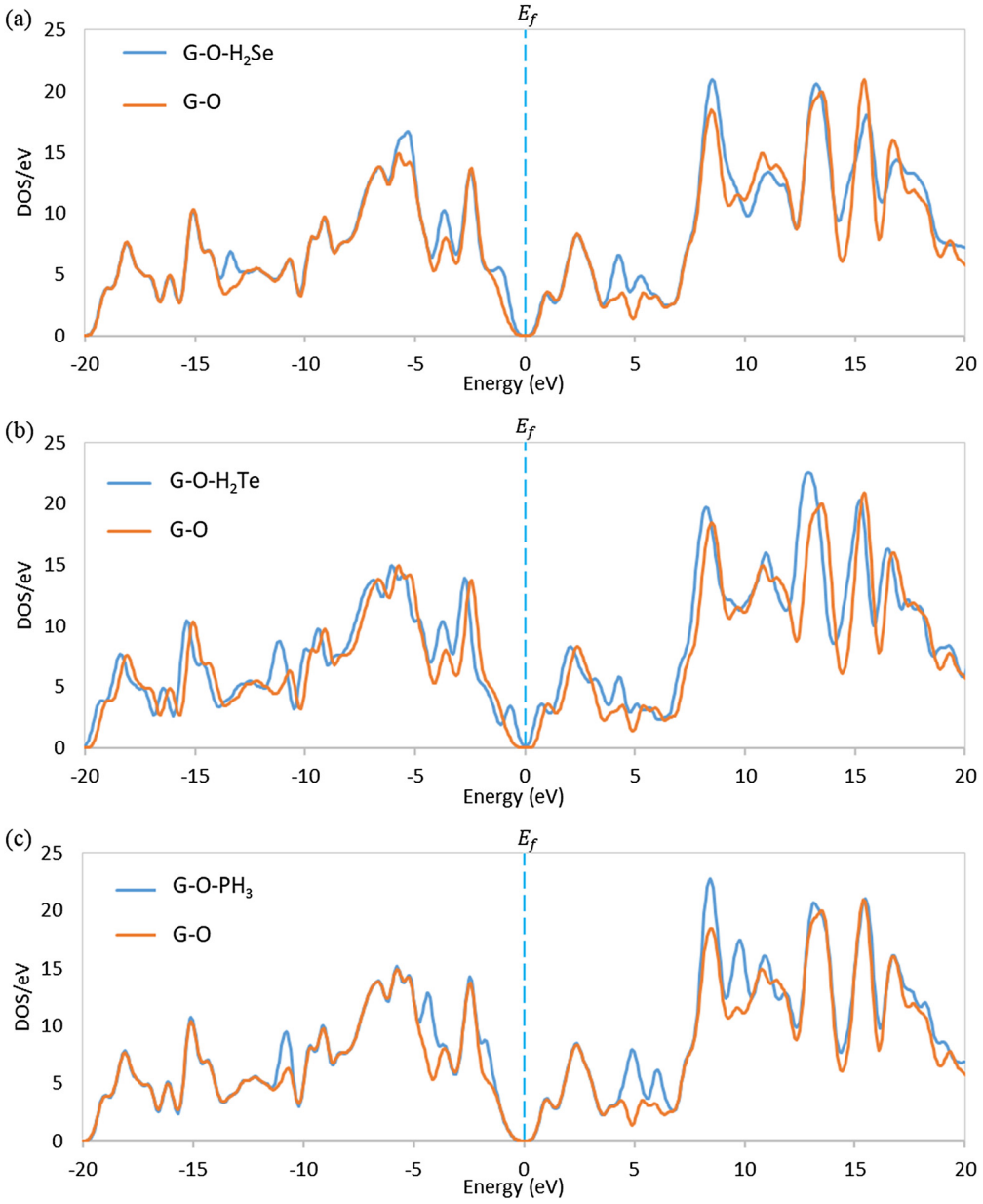

Fig. 5. Density of states of G–O system prior and after the adsorption of a) H_2Se, b) H_2Te, and c) PH_3.

changes of the DOS of G–O upon the adsorption of H_2Se, H_2Te, and PH_3 molecules are shown in Figs. 5(a)–5(c). For instance, a considerable increase in the DOS around −13.3 −5.2, −3.6, 4.3, 5.4, and 8.6 eV is observed after the adsorption of H_2Se. For the case of H_2Te (Fig. 5(b)), a significant increase of DOS around −3.6 and 4.4 eV is observed. The two peaks around −10.5 and 13.5 eV shift to −11.1 and 13.0 eV, respectively, with higher intensity. Besides, a new peak around −0.5 eV is observed as well upon the adsorption of gas molecule. Furthermore, a significant increase in the DOS around −10.7, 6.2, 8.2, and 9.7 eV, as well as two new peaks around −4.3 and 4.7 eV are detected after the adsorption of PH_3.

3.3. Functionalization with hydroxyl group (G–OH)

In this part, the surface of G is functionalized with –OH group to form G–OH and then utilized as a gas sensor to detect H_2Se, H_2Te, and PH_3 molecules. G–OH with and without the H_2Se, H_2Te, and PH_3 molecules are firstly optimized to reach the most stable adsorption configuration. Figs. 1(i)–1(l) show the most stable configuration of G–OH before and after the adsorption of the gas molecules. The results show that, the C–O and O–H bonds are 1.5 Å and 0.98 Å, respectively, and the C–C bond close to the –OH group increases to 1.5 Å. Table 1 shows the adsorption energy, adsorption distance as well as the charge transfer between G–OH and H_2Se, H_2Te, and PH_3 molecules. A remarkable increase in adsorption energy with −0.244 eV as well as charge transfer with −0.097 e is observed for the case of H_2Se adsorbed on G–OH as compared with G. Moreover, the adsorption distance decreases to 2.19 Å reflecting an improvement in the sensitivity of G–OH toward the sensing of H_2Se. An increase in the adsorption energy to −0.170 and −0.124 eV is also observed for the cases of H_2Te and PH_3, respectively. Figs. 6(a)–6(d) show the band structures of G–OH prior and after gas adsorption of H_2Se, H_2Te, and PH_3 molecules. Fig. 6(a) shows that a new band is detected at the Fermi level making the band gap equal to zero upon the functionalization with –OH group. Moreover, some changes and new bands are observed beneath and above the Fermi level af-

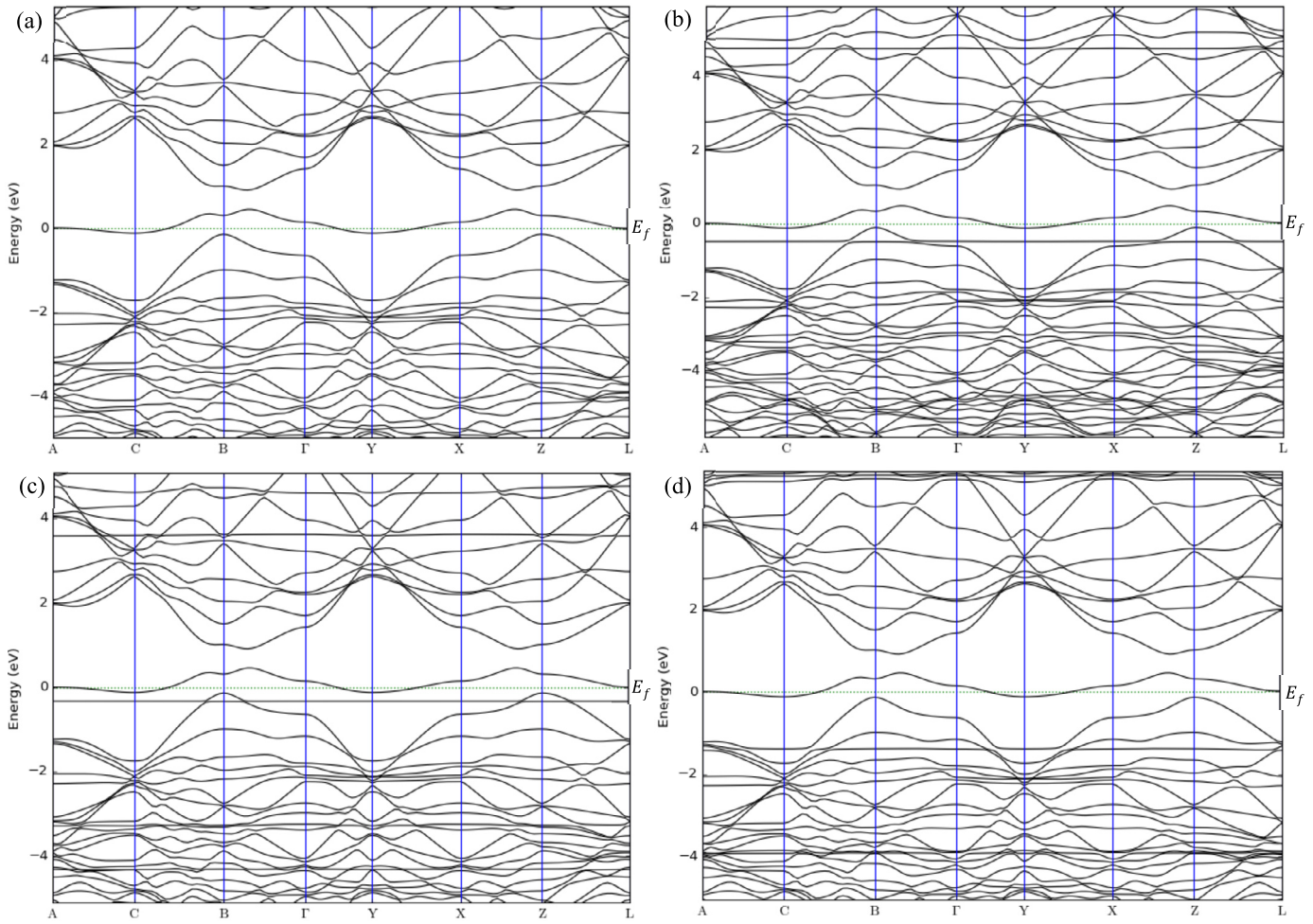

Fig. 6. Band structures of a) G–OH, b) G–OH–H_2Se, c) G–OH–H_2Te, and d) G–OH–PH_3.

ter the adsorption of H_2Se, H_2Te, and PH_3 molecules as shown in Figs. 6(b)–6(d). The band structure results are then confirmed by the DOS results in Figs. 7(a)–7(c). As shown in Fig. 7(a), a new peak is observed at the Fermi level which confirms the zero band gap as well as the appearance of new bands at Fermi level as shown in the band structures of G–OH. The presence of this new peak is attributed to the improvement in the conductivity of G–OH upon the functionalization with –OH group. After adsorption of H_2Se, a considerable increase in the DOS around −12.8, −4.7, −3.1, and 10.1 eV is observed. The two peaks around 5.7 and 6.9 eV shift to 4.9 and 6.4 eV with higher intensity. Moreover, the peak at the Fermi level increases and shifts slightly to −0.2 eV. For the case of H_2Te (Fig. 6(b)), a significant increase in the DOS around −3.2, 4.6, and 9.0 eV is observed. A new peak also appears around −10.8 eV and a significant increase in the peak at Fermi level is observed. Furthermore, upon adsorption of PH_3, an increase in the DOS around −10.3, −3.9, 5.5, 6.7, 8.9, and 10.2 eV is observed.

3.4. Functionalization with both epoxy and hydroxyl groups (G–O–OH)

To investigate further the sensitivity, the surface of G is functionalized using –O– and –OH groups to form G–O–OH system. The stable configuration of G–O–OH prior and after the adsorption of the H_2Se, H_2Te, and PH_3 molecules are shown in Figs. 1(m)–1(p). The adsorption energy, charge transfer, as well as adsorption distance of the optimized H_2Se, H_2Te, and PH_3 molecules adsorbed on G–O–OH are calculated and listed in Table 1. The results show that the adsorption parameters are significantly improved upon the functionalization of G with both –O– and –OH groups. For instance, the adsorption energy rises to −0.265 eV, the adsorption distance drops to 2.39 Å, and the charge transfer increases significantly to −0.113 for the case of H_2Se gas. The same behavior is observed as well for the cases of H_2Te and PH_3 molecules. Figs. 8(a)–8(d) show the band structures of G–O–OH prior and after the adsorption H_2Se, H_2Te, and PH_3 molecules. Although, no changes are detected in the band gap, some changes and new bands are noticed beneath and above Fermi level after the adsorption of H_2Se, H_2Te, and PH_3 molecules as shown in Figs. 8(b)–8(d). Figs. 9(a)–9(c) show the DOS of G–O–OH prior and after the adsorption of H_2Se, H_2Te, and PH_3 molecules. Fig. 9(a) shows that a new peak is observed at the Fermi level confirming the band structure results of G–O–OH. Upon the adsorption of H_2Se, an increase in the DOS at around −12.8, −5.0, −3.1, 4.8, 9.9, and 13.6 eV is observed. In addition, a new peak is observed around 6.4 eV. A considerable increase in the DOS around −10.6, −4.2, −3.2, 3.9, 4.6, 16.9, and 19.4 eV is observed for the case of H_2Te (Fig. 9(b)). The two peaks around 11.0 and 11.8 eV disappear and a new peak with higher intensity appears around 11.5 eV. Moreover, a significant increase in the peak at Fermi level is also observed. For the case of PH_3, a remarkable increase in the DOS around −10.3, −3.9, 5.5, 6.7, 8.9, 10.0, and 17.9 eV is observed.

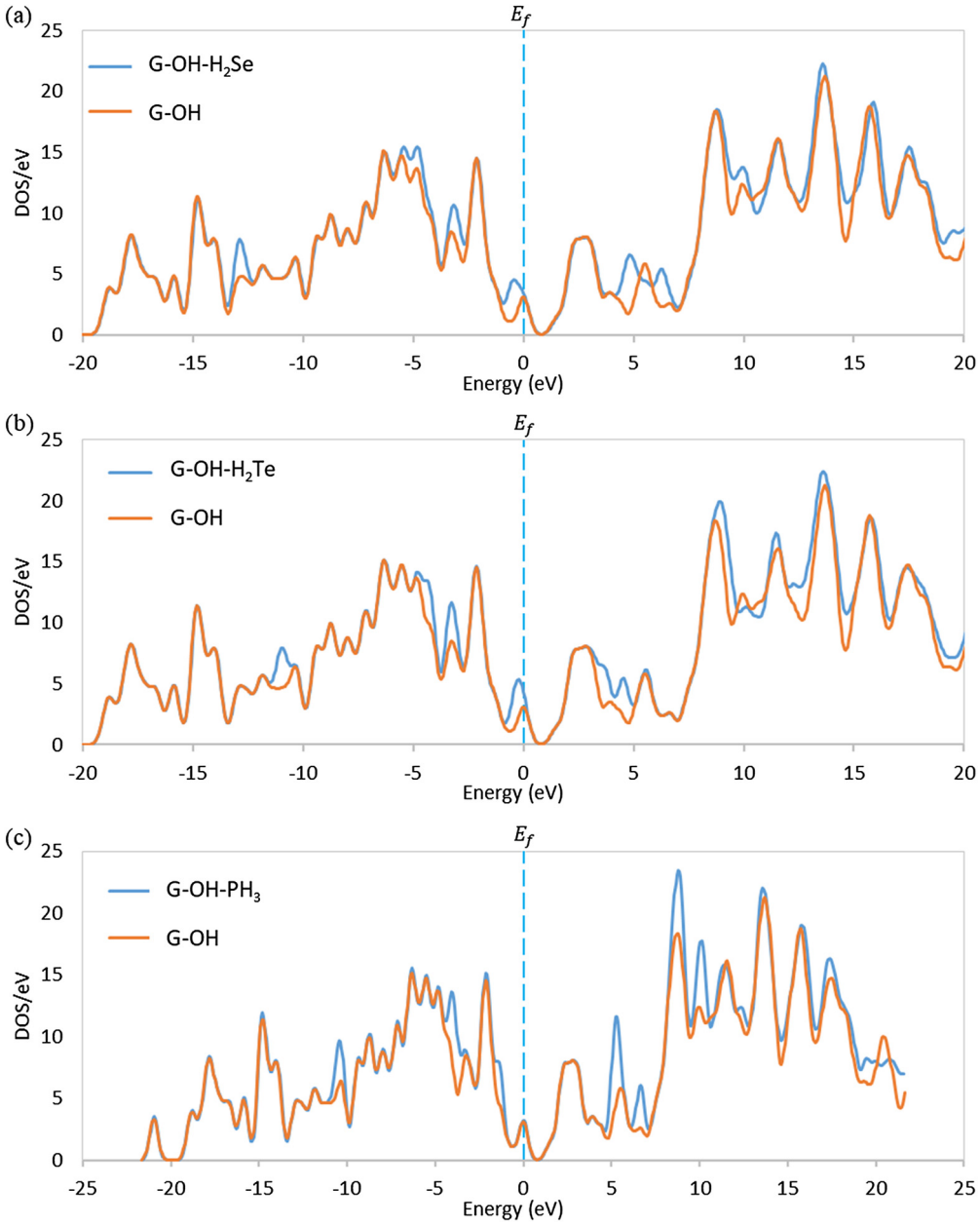

Fig. 7. Density of states of G–OH system before and after the adsorption of a) H_2Se, b) H_2Te, and c) PH_3.

3.5. Discussion

Different theoretical studies have been reported in the recent years about functionalizing G-based materials with –O– and –OH functional groups for the purpose of improving their sensitivity for the field of gas sensors [52–55]. For example, graphene was functionalized with –OH group and used to detect H_2S gas [52]. The researchers of this study demonstrated that the adsorption energy of graphene was improved significantly upon functionalizing its surface with –OH group. Very recently, three different G-based materials (GNS, AGNR, and ZGNR) were functionalized with –O– and –OH groups and then used as a gas sensor to detect H_2S gas [56]. The results of this study revealed that the sensing performance of the built systems was remarkably improved after functionalizing their surface with –O– and –OH functional groups. Those investigations revealed that functionalization of graphene with O– and –OH groups increase its efficiency towards adsorption of polar gases. Furthermore, some other materials have been used recently to detect H_2Se, H_2Te, and PH_3 molecules. For example, Cl functionalized aluminum nitride and aluminum phosphide nanocone sheets were utilized based on density functional theory as a gas sensor to detect H_2Se [57]. The results of this study showed that the adsorption energy for the case of H_2Se adsorbed on aluminum phosphide nanocone sheets was higher than the case of aluminum nitride. In another study, V_2O_5(0 0 1) surface has been used to detect H_2Se, H_2Te, and PH_3 molecules in addition to some other gases [58]. The researchers of this work showed that the vanadium atom played a significant role in the adsorption process of the target molecules.

The remarkable improvement of the adsorption parameters and hence the sensitivity of GO is obtained thanks to the existence of –O– and –OH functional groups that were reported to facilitate the gas adsorption [26,35,36]. After optimization of gas molecules, each molecule reorients itself based on its reactivity at a certain

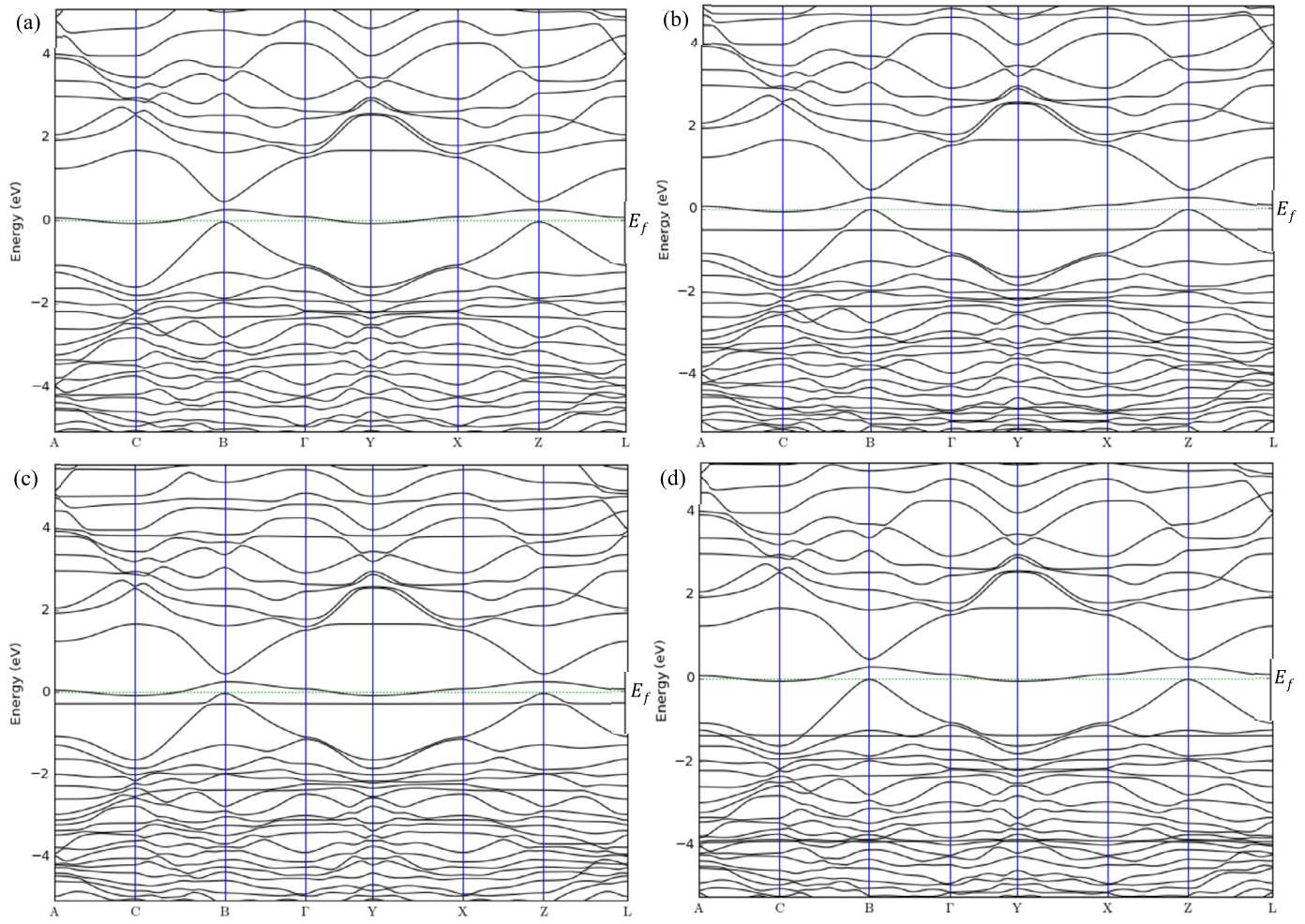

Fig. 8. Band Structures of a) G–O–OH, b) G–O–OH–H_2Se, c) G–O–OH–H_2Te, and d) G–O–OH–PH_3.

distance from G and GO, known as adsorption distance [50]. For the case of G shown in Figs. 1(b)–1(d), the H_2Se, H_2Te, and PH_3 molecules reorient themselves in which the selenide atom of H_2Se and two hydrogen atoms of PH_3 located close to the G plane while for the largest molecule H_2Te becomes almost parallel to the surface plane of G. For the cases of G–O, G–OH, and G–O–OH shown in Figs. 1(e)–1(p), the gas molecules reorient themselves in which the hydrogen atoms become closer to the oxygen atoms of –O– and –OH groups with much smaller adsorption distances as compared with G. The obtained configurations indicate that the adsorption may take place among the hydrogen atoms of the H_2Se, H_2Te, and PH_3 molecules and the oxygen atoms of –O– and –OH groups. The charge transfer can be discussed using the hybridization principle of the HOMO and LUMO for adsorbate molecules along through surface states following reference [59]. Herein, mixing the HOMO adsorbates with surface states overhead Fermi level for the adsorbent cause charge transfer to the surface from the molecule. The involvement of the LUMO for gas molecule of occupied states of the surface causes charge transmission from the surface to the gas molecule. These processes happen if the considered orbitals are close energy levels and they include non-zero overlap. The significant increase in the density of states after the adsorption of H_2Se, H_2Te, and PH_3 molecules demonstrating that more number of states become available to be occupied upon the adsorption of gas molecules which confirm the successful detection of H_2Se, H_2Te, and PH_3 molecules [50]. Furthermore, the appearance of new bands in the band structures as well as the increase in the DOS at Fermi level are indications of the improvement of G and GO conductivity upon the adsorption of H_2Se, H_2Te, and PH_3 molecules which is in rational agreement with the reported literature [60–62]. The sensing mechanism of H_2Se and H_2Te adsorption on G–OH and G–O–OH systems can be described using the following equation [63]:

$$H_2X + OH \rightarrow XH + H_2O \quad (2)$$

with X is either Se or Te. The surface potential energy for the $H_2X + OH$ reaction was tested and demonstrated its ability [63]. The adsorption energy of PH_3 is expected to be high since the P atom has high electron density. However, the main factors that determine the efficiency of gas adsorption are its electronegativity and dipole moment [64]. Therefore, the above systems are more efficient for H_2Se adsorption.

Fig. 10 shows a comparison between the adsorption parameters of the optimized H_2Se, H_2Te, and PH_3 molecules adsorbed on the surface of G, G–O, G–OH, and G–O–OH systems. The calculations show that functionalizing the surface of G to create GO improved the adsorption parameters. Particularly, the adsorption energy, charge transfer as well as adsorption distance between the three different forms of GO and H_2Se significantly enhanced as compared with the other two gases. These results indicate that GO is more selective to H_2Se gas than for the cases of H_2Te and PH_3.

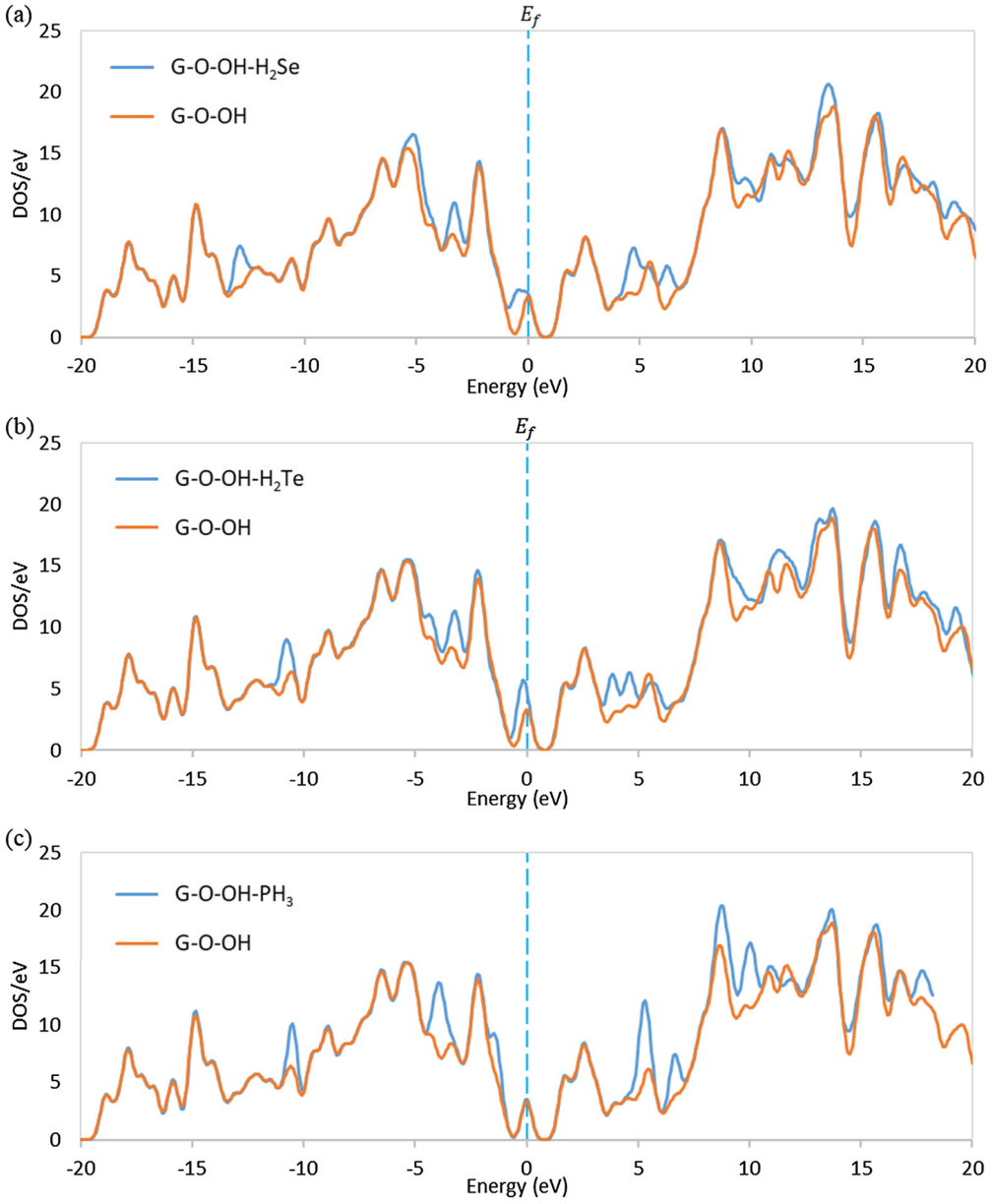

Fig. 9. Density of states of G–O–OH system before and after the adsorption of a) H_2Se, b) H_2Te, and c) PH_3.

4. Conclusion

In this paper, first principles investigations of the H_2Se, H_2Te, and PH_3 molecules adsorption on the surface of graphene (G) and graphene oxide (GO) have been reported. The obtained results show that, G was capable to detect the gas molecules. For instance, the highest adsorption energy was found for the case of H_2Te with −0.143 eV, the smallest adsorption distance was found for the case of PH_3 with 3.41 Å, and the highest charge transfer with −0.011 e was found for the case of PH_3. To enhance the sensitivity, the surface of G is then functionalized with –O– and –OH functional groups to form: G–O, G–OH, and G–O–OH. The adsorption energies, adsorption distances as well as charge transfer have been significantly enhanced upon the functionalization. The highest adsorption energy with −0.319 eV as well as the smallest adsorption distance with 2.28 Å were observed for the case of H_2Se adsorbed on G–O. In addition, the highest charge transfer was found for the case of H_2Se adsorbed on G–O–OH with −0.113 e. Those results confirm that functionalization of the surface of G with –O– and –OH functional groups leads to advance its sensitivity for the application of gas sensors.

Declaration of competing interest

The authors declare that they have no known competing financial interests or personal relationships that could have appeared to influence the work reported in this paper.

Acknowledgements

The publication of this article was funded by the Qatar National Library.

References

[1] S. Aghaei, M. Monshi, I. Calizo, A theoretical study of gas adsorption on silicene nanoribbons and its application in a highly sensitive molecule sensor, RSC Adv. 6 (2016) 94417–94428.

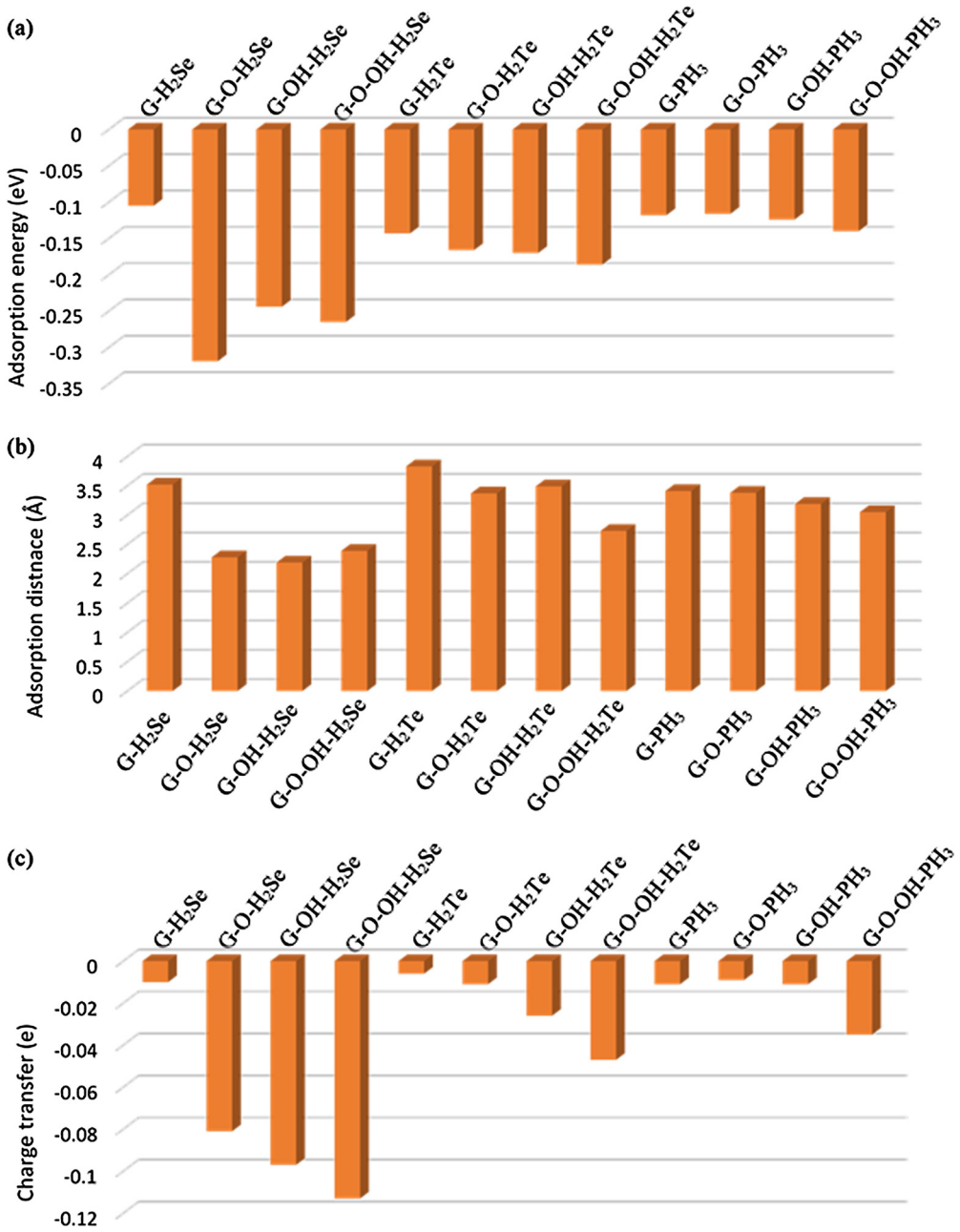

Fig. 10. Comparison between the a) adsorption energy, b) adsorption distance, and c) charge transfer of the optimized H_2Se, H_2Te, and PH_3 molecules adsorbed on G, G–O, G–OH, and G–O–OH.

[2] H. Liu, W. Zhu, Y. Han, Z. Yang, Y. Huang, Single-nanowire fuse for ionization gas detection, Sensors 19 (2019) 4358.

[3] A.I. Ayesh, A.A. Alyafei, R.S. Anjum, R.M. Mohamed, M.B. Abuharb, B. Salah, M. El-Muraikhi, Production of sensitive gas sensors using CuO/SnO_2 nanoparticles, Appl. Phys. A 125 (2019) 550.

[4] B. Malczewska-Toth, Phosphorus, selenium, tellurium, and sulfur, in: Patty's Toxicology, 2001, pp. 841–884.

[5] S.M. Abrishamifar, N. Heidari, R. Razavi, M.J. Lariche, M. Najafi, The Cl functionalized aluminum nitride (AlN) and aluminum phosphide (AlP) nanocone sheets as hydrogen selenide (H2Se) sensor: a density functional investigation, Acta Chim. Slov. 65 (2018) 208–212.

[6] A. Zwart, J. Arts, W. Ten Berge, L. Appelman, Alternative acute inhalation toxicity testing by determination of the concentration-time-mortality relationship: experimental comparison with standard LC50 testing, Regul. Toxicol. Pharmacol. 15 (1992) 278–290.

[7] F. Xin, Y. Tian, X. Zhang, Ratiometric fluorescent probe for highly selective detection of gaseous H2Se, Dyes Pigments 177 (2020) 108274.

[8] B. Berck, Sorption of phosphine by cereal products, J. Agric. Food Chem. 16 (1968) 419–425.

[9] R. Bhuvaneswari, V. Nagarajan, R. Chandiramouli, Arsenene nanoribbons for sensing NH3 and PH3 gas molecules–a first-principles perspective, Appl. Surf. Sci. 469 (2019) 173–180.

[10] A.A. Peyghan, S.F. Rastegar, N.L. Hadipour, DFT study of NH3 adsorption on pristine, Ni- and Si-doped graphynes, Phys. Lett. A 378 (2014) 2184–2190.

[11] A.A. Peyghan, Z. Bagheri, Electronic response of BC3 nanotube to CS2 molecules: DFT studies, Comput. Theor. Chem. 1008 (2013) 1–7.

[12] H.J. Yoon, J.H. Yang, Z. Zhou, S.S. Yang, M.M.-C. Cheng, Carbon dioxide gas sensor using a graphene sheet, Sens. Actuators B, Chem. 157 (2011) 310–313.

[13] A.A. Peyghan, M. Noei, M.B. Tabar, A large gap opening of graphene induced by the adsorption of Co on the Al-doped site, J. Mol. Model. 19 (2013) 3007–3014.

[14] M.M. Monshi, S.M. Aghaei, I. Calizo, Doping and defect-induced germanene: a superior media for sensing H2S, SO2, and CO2 gas molecules, Surf. Sci. 665 (2017) 96–102.

[15] A.I. Ayesh, A.F. Abu-Hani, S.T. Mahmoud, Y. Haik, Selective H2S sensor based on CuO nanoparticles embedded in organic membranes, Sens. Actuators B, Chem. 231 (2016) 593–600.

[16] M.A. Haija, A.F. Abu-Hani, N. Hamdan, S. Stephen, A.I. Ayesh, Characterization of H2S gas sensor based on CuFe2O4 nanoparticles, J. Alloys Compd. 690 (2017) 461–468.

[17] J. Van Lith, A. Lassesson, S. Brown, M. Schulze, J. Partridge, A. Ayesh, A hydrogen sensor based on tunneling between palladium clusters, Appl. Phys. Lett. 91 (2007) 181910.
[18] Y.-H. Zhang, Y.-B. Chen, K.-G. Zhou, C.-H. Liu, J. Zeng, H.-L. Zhang, Y. Peng, Improving gas sensing properties of graphene by introducing dopants and defects: a first-principles study, Nanotechnology 20 (2009) 185504.
[19] A. Hosseinian, Z. Asadi, L. Edjlali, A. Bekhradnia, E. Vessally, NO2 sensing properties of a borazine doped nanographene: a DFT study, Comput. Theor. Chem. 1106 (2017) 36–42.
[20] F.R. Baptista, S. Belhout, S. Giordani, S. Quinn, Recent developments in carbon nanomaterial sensors, Chem. Soc. Rev. 44 (2015) 4433–4453.
[21] I.M. El-Sherbiny, E. Salih, Green synthesis of metallic nanoparticles using biopolymers and plant extracts, in: Green Metal Nanoparticles: Synthesis, Characterization and Their Applications, 2018, p. 293.
[22] G. Lu, K. Yu, L.E. Ocola, J. Chen, Ultrafast room temperature NH3 sensing with positively gated reduced graphene oxide field-effect transistors, Chem. Commun. 47 (2011) 7761–7763.
[23] X. Huang, N. Hu, R. Gao, Y. Yu, Y. Wang, Z. Yang, E.S.-W. Kong, H. Wei, Y. Zhang, Reduced graphene oxide–polyaniline hybrid: preparation, characterization and its applications for ammonia gas sensing, J. Mater. Chem. 22 (2012) 22488–22495.
[24] R.K. Paul, S. Badhulika, N.M. Saucedo, A. Mulchandani, Graphene nanomesh as highly sensitive chemiresistor gas sensor, Anal. Chem. 84 (2012) 8171–8178.
[25] A. Salehi-Khojin, D. Estrada, K.Y. Lin, M.H. Bae, F. Xiong, E. Pop, R.I. Masel, Polycrystalline graphene ribbons as chemiresistors, Adv. Mater. 24 (2012) 53–57.
[26] S.G. Chatterjee, S. Chatterjee, A.K. Ray, A.K. Chakraborty, Graphene–metal oxide nanohybrids for toxic gas sensor: a review, Sens. Actuators B, Chem. 221 (2015) 1170–1181.
[27] A.N.A. Anasthasiya, M. Khaneja, B. Jeyaprakash, Electronic structure calculations of ammonia adsorption on graphene and graphene oxide with epoxide and hydroxyl groups, J. Electron. Mater. 46 (2017) 5642–5656.
[28] L. Shao, G. Chen, H. Ye, H. Niu, Y. Wu, Y. Zhu, B. Ding, Sulfur dioxide molecule sensors based on zigzag graphene nanoribbons with and without Cr dopant, Phys. Lett. A 378 (2014) 667–671.
[29] B. Manna, H. Raha, I. Chakrabarti, P.K. Guha, Selective reduction of oxygen functional groups to improve the response characteristics of graphene oxide-based formaldehyde sensor device: a first principle study, IEEE Trans. Electron Devices 65 (2018) 5045–5052.
[30] Y. Wan, Y. Wang, J. Wu, D. Zhang, Graphene oxide sheet-mediated silver enhancement for application to electrochemical biosensors, Anal. Chem. 83 (2011) 648–653.
[31] E. Salih, M. Mekawy, R.Y. Hassan, I.M. El-Sherbiny, Synthesis, characterization and electrochemical-sensor applications of zinc oxide/graphene oxide nanocomposite, J. Nanostruct. Chem. 6 (2016) 137–144.
[32] I. Kuznetsova, V. Kolesov, B. Zaitsev, S. Tkachev, V. Kashin, A. Shikhabudinov, A. Fionov, S. Gubin, S. Sun, Structural, electrical, and acoustical properties of graphene oxide films for acoustoelectronic applications, Phys. Status Solidi A 214 (2017) 1600757.
[33] M.-H. Wang, Q. Li, X. Li, Y. Liu, L.-Z. Fan, Effect of oxygen-containing functional groups in epoxy/reduced graphene oxide composite coatings on corrosion protection and antimicrobial properties, Appl. Surf. Sci. 448 (2018) 351–361.
[34] J. Qiu, D. Wang, H. Geng, J. Guo, S. Qian, X. Liu, How oxygen-containing groups on graphene influence the antibacterial behaviors, Adv. Mater. Interfaces 4 (2017) 1700228.
[35] K. Toda, R. Furue, S. Hayami, Recent progress in applications of graphene oxide for gas sensing: a review, Anal. Chim. Acta 878 (2015) 43–53.
[36] Y. Peng, J. Li, Ammonia adsorption on graphene and graphene oxide: a first-principles study, Front. Environ. Sci. Eng. 7 (2013) 403–411.
[37] J.S. Cho, S.Y. Lee, J.-K. Lee, Y.C. Kang, Iron telluride-decorated reduced graphene oxide hybrid microspheres as anode materials with improved Na-ion storage properties, ACS Appl. Mater. Interfaces 8 (2016) 21343–21349.
[38] J. Wang, B. Singh, J.-H. Park, S. Rathi, I.-y. Lee, S. Maeng, H.-I. Joh, C.-H. Lee, G.-H. Kim, Dielectrophoresis of graphene oxide nanostructures for hydrogen gas sensor at room temperature, Sens. Actuators B, Chem. 194 (2014) 296–302.
[39] Y.R. Choi, Y.-G. Yoon, K.S. Choi, J.H. Kang, Y.-S. Shim, Y.H. Kim, H.J. Chang, J.-H. Lee, C.R. Park, S.Y. Kim, Role of oxygen functional groups in graphene oxide for reversible room-temperature NO2 sensing, Carbon 91 (2015) 178–187.
[40] J.P. Perdew, K. Burke, M. Ernzerhof, Generalized gradient approximation made simple, Phys. Rev. Lett. 77 (1996) 3865.
[41] S. Grimme, Semiempirical GGA-type density functional constructed with a long-range dispersion correction, J. Comput. Chem. 27 (2006) 1787–1799.
[42] H.J. Monkhorst, J.D. Pack, Special points for Brillouin-zone integrations, Phys. Rev. B 13 (1976) 5188.
[43] W. Gao, P. Xiao, G. Henkelman, K.M. Liechti, R. Huang, Interfacial adhesion between graphene and silicon dioxide by density functional theory with van der Waals corrections, J. Phys. D, Appl. Phys. 47 (2014) 255301.
[44] D. Liu, Y. Gui, C. Ji, C. Tang, Q. Zhou, J. Li, X. Zhang, Adsorption of SF6 decomposition components over Pd (1 1 1): a density functional theory study, Appl. Surf. Sci. 465 (2019) 172–179.
[45] J. Neugebauer, M. Scheffler, Adsorbate-substrate and adsorbate-adsorbate interactions of Na and K adlayers on Al (111), Phys. Rev. B 46 (1992) 16067.
[46] Z. Bo, X. Guo, X. Wei, H. Yang, J. Yan, K. Cen, Density functional theory calculations of NO2 and H2S adsorption on the group 10 transition metal (Ni, Pd and Pt) decorated graphene, Physica E, Low-Dimens. Syst. Nanostruct. 109 (2019) 156–163.
[47] R.S. Mulliken, Electronic population analysis on LCAO–MO molecular wave functions. I, J. Chem. Phys. 23 (1955) 1833–1840.
[48] Y. Taluja, B. SanthiBhushan, S. Yadav, A. Srivastava, Defect and functionalized graphene for supercapacitor electrodes, Superlattices Microstruct. 98 (2016) 306–315.
[49] V.E.C. Padilla, M.T.R. de la Cruz, Y.E.Á. Alvarado, R.G. Díaz, C.E.R. García, G.H. Cocoletzi, Studies of hydrogen sulfide and ammonia adsorption on P- and Si-doped graphene: density functional theory calculations, J. Mol. Model. 25 (2019) 94.
[50] G.K. Walia, D.K.K. Randhawa, First-principles investigation on defect-induced silicene nanoribbons—a superior media for sensing NH3, NO2 and NO gas molecules, Surf. Sci. 670 (2018) 33–43.
[51] A.S. Dobrota, I.A. Pašti, N.V. Skorodumova, Oxidized graphene as an electrode material for rechargeable metal-ion batteries–a DFT point of view, Electrochim. Acta 176 (2015) 1092–1099.
[52] X. Gao, Q. Zhou, J. Wang, L. Xu, W. Zeng, Performance of intrinsic and modified graphene for the adsorption of H2S and CH4: a DFT study, Nanomaterials 10 (2020) 299.
[53] I. Maity, K. Ghosh, H. Rahaman, P. Bhattacharyya, Selectivity tuning of graphene oxide based reliable gas sensor devices by tailoring the oxygen functional groups: a DFT study based approach, IEEE Trans. Device Mater. Reliab. 17 (2017) 738–745.
[54] E. Salih, A.I. Ayesh, CO, CO2, and SO2 detection based on functionalized graphene nanoribbons, in: First Principles Study, Physica E, Low-Dimens. Syst. Nanostruct. (2020) 114220.
[55] E. Salih, A.I. Ayesh, Enhancing the sensing performance of zigzag graphene nanoribbon to detect NO, NO2, and NH3 gases, Sensors 20 (2020).
[56] E. Salih, A.I. Ayesh, DFT investigation of H2S adsorption on graphene nanosheets and nanoribbons: comparative study, Superlattices Microstruct. 146 (2020) 106650, https://doi.org/10.1016/j.spmi.2020.106650.
[57] S.M. Abrishamifar, N. Heidari, R. Razavi, M.J. Lariche, M. Najafi, The Cl functionalized aluminum nitride (AlN) and aluminum phosphide (AlP) nanocone sheetsas hydrogen selenide (H 2 Se) sensor: a density functional investigation, Acta Chim. Slov. 65 (2018) 208–212.
[58] V.A. Ranea, P.L.D. Quiña, N.M. Yalet, General adsorption model for H2S, H2Se, H2Te, NH3, PH3, AsH3 and SbH3 on the V2O5 (0 0 1) surface including the van der Waals interaction, Chem. Phys. Lett. 720 (2019) 58–63.
[59] M.Y. Notash, A.R. Ebrahimzadeh, Van der Waals corrected DFT study of adsorption of groups VA and VIA hydrides on graphene monoxide, Physica E, Low-Dimens. Syst. Nanostruct. 80 (2016) 202–206.
[60] G. Ko, H.-Y. Kim, J. Ahn, Y.-M. Park, K.-Y. Lee, J. Kim, Graphene-based nitrogen dioxide gas sensors, Curr. Appl. Phys. 10 (2010) 1002–1004.
[61] M.T. Ahmadi, R. Ismail, S. Anwar, Handbook of Research on Nanoelectronic Sensor Modeling and Applications, IGI Global, 2016.
[62] E. Akbari, A. Afroozeh, M.L.P. Tan, V.K. Arora, M. Ghadiry, Analytical assessment of carbon allotropes for gas sensor applications, Measurement 92 (2016) 295–302.
[63] M. Tang, X. Chen, Y. Xie, H.F. Schaefer, Hydrogen abstraction reaction H2Se + OH → H2O + SeH: comparison with the analogous hydrogen sulfide and water reactions, Inorg. Chem. 58 (2019) 2069–2079.
[64] P. Snehha, V. Nagarajan, R. Chandiramouli, Novel bismuthene nanotubes to detect NH3, NO2 and PH3 gas molecules – a first-principles insight, Chem. Phys. Lett. 712 (2018) 102–111.